Development and validation of a predictive combustion model for hydrogen-fuelled internal combustion engines

International Journal of Hydrogen Energy 89 (2024) 1310–1320

Contents lists available at ScienceDirect

International Journal of Hydrogen Energy

journal homepage: www.elsevier.com/locate/he

Development and validation of a predictive combustion model for hydrogen-fuelled internal combustion engines

Andrea Piano [a,*], Gianpaolo Quattrone [a], Federico Millo [a], Francesco Pesce [b], Alberto Vassallo [b]

[a] Politecnico di Torino, Energy Department, Torino, Italy
[b] Dumarey Automotive Italia SpA, Torino, Italy

ARTICLE INFO

Handling Editor: Dr F Gallucci

Keywords:
Hydrogen
Internal combustion engine
Alternative fuels
Modelling

ABSTRACT

Internal combustion engines (ICEs) fuelled with hydrogen can play a major role in the short-term future transportation sector since they abate all criteria pollutants at engine-out reducing tailpipe CO2 emissions to near-zero levels. However, optimizing hydrogen ICEs is a challenging task that can be addressed through the development of a robust simulation tool capable to predict the H2 combustion process. In this study, a previously developed two-zone combustion model has been updated considering different laminar flame speed computations, both based on a detailed chemistry scheme: a polynomial correlation function and a tabulated approach. The predictive capabilities of the combustion model have been validated against experimental data coming from a 0.5L PFI single-cylinder engine under several operating conditions. The tabulated approach for laminar flame speed definition proved to be the best solution, leading to a combustion duration average error lower than 3 deg over a dataset containing more than 45 different operating conditions.

1. Introduction

In order to achieve the highly ambitious carbon emission targets set within the framework of the Net Zero Emissions by 2050 (NZE) scenario [1], several OEMs in the transportation sector have introduced a range of innovative solutions. Besides the transition to battery electric vehicles (BEVs) and hydrogen fuel cells (FCEVs) for light-duty applications, the utilization of low-emissions fuels such as biofuels, e-fuels, and hydrogen in internal combustion engines is gaining significant momentum [2,3]. Among them, hydrogen can be produced using renewable energy sources [4], and its complete combustion does not produce GHG emissions due to its zero carbon content. Moreover, hydrogen has physical peculiarities that make its usage as a fuel for ICEs particularly appealing [5]. In particular, it is noteworthy that hydrogen is characterized by a higher Lower Heating Value (LHV) in comparison with the traditional fossil fuels commonly used for internal combustion engines (i.e., H2 = 120 MJ/kg vs Gasoline = 44.1 MJ/kg [6]). Moreover, hydrogen features high flame speed propagation over a wide range of temperatures, pressure, and air-to-fuel ratios [7], which makes it particularly suitable for lean combustion strategies, extending the usual flammability limits. Lean combustion strategies are indeed beneficial for engine thermal efficiency, due to the reduced heat rejection [2] and the low pumping losses typical of unthrottled operations [8]. Several studies in literature [9,10] show that hydrogen has a good combustion stability even with high excess air ratios, retaining the coefficient of variation of the indicated mean effective pressure (COV IMEP) lower than 3%. In addition, mixture enleanment is beneficial for reducing the NOx emission to extremely low levels [11], thanks to the low in-cylinder temperatures. Lean combustion strategies are commonly employed even at high loads, allowing to achieve higher levels of brake mean effective pressure (BMEP) without incurring in abnormal combustion events, compared to stoichiometric conditions [12]. However, despite the high auto-ignition temperature and the high Research Octane Number (RON) [13], hot spots or residuals in the combustion chamber can easily ignite hydrogen-air mixtures due to their low minimum ignition energy (at stoichiometry, 0.02 mJ compared to 0.25 mJ of Gasoline [13]). In light of all the peculiarities that characterize the air-hydrogen mixtures combustion, the development of hydrogen-fuelled internal combustion engine is gaining high interest, moving the focus of the OEMs towards the development of such concepts. In this framework, the availability of combustion models able to predict the average pressure cycle for premixed hydrogen-air mixtures can be extremely important to support the engine development process. To this aim, several predictive models have been proposed in literature. D'Errico et al. [14] presented a

* Corresponding author.
E-mail address: andrea.piano@polito.it (A. Piano).

https://doi.org/10.1016/j.ijhydene.2024.09.407
Received 6 August 2024; Received in revised form 19 September 2024; Accepted 28 September 2024

Table 1
Main characteristics of the single cylinder engine.

Bore	83 mm
Stroke	90.4 mm
Displacement	0.5 L
CR	12
Piston Type	Hemi-spherical bowl
Fuel System	PFI with rail with relative feed pressure 6–8 bar

Table 2
Limits of the main operating parameters varied throughout the experimental campaign.

Parameter	Full Load		Partial Load	
	Lower Limit	Upper Limit	Lower Limit	Upper Limit
Spark Advance [CAD bTDCf]	>5	<35	>0	<35
Lambda [−]	>1.3	<2.3	>1.3	<2.5
Boost Pressure [bar]	>2.5	<3.5	>1.1	<1.8
EGR [%]	0	<15	0	<15

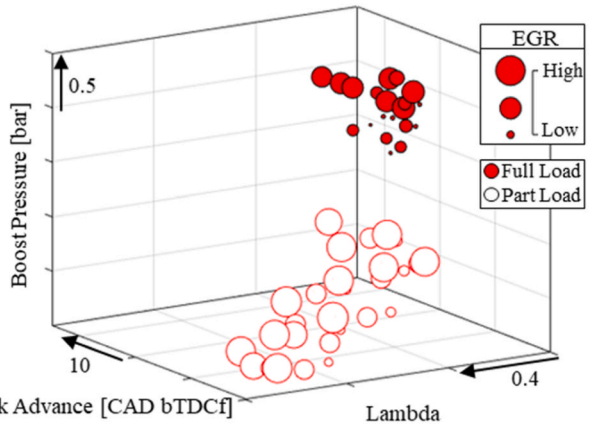

Fig. 1. Experimental test matrix.

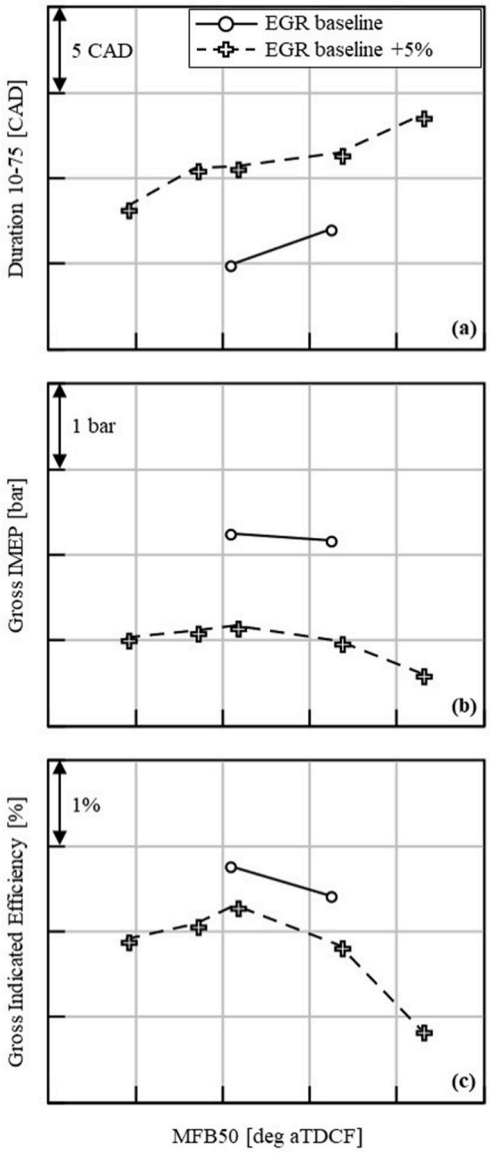

Fig. 2. Experimental data regarding two spark advance sweeps performed at EGR "baseline" and EGR "baseline" +5% – full load conditions.

quasi-dimensional predictive model for hydrogen combustion with cryogenic port injection. In this study, the laminar flame speed was calculated through detailed chemistry calculations based on an in-house reaction scheme over a wide range of engine-relevant operating conditions. The laminar flame speed model was implemented into the combustion model through a correlation function whose coefficients were tuned to minimize the standard deviation with respect to the detailed chemistry results. The combustion model provided results consistent with the experimental data but showed some discrepancies at operating points with (very) lean mixtures. Rezaei et al. [15] presented a phenomenological model for the prediction of hydrogen combustion. The model is based on the renowned SITurb model, provided by the commercial software GT-SUITE, largely employed in several studies [16, 17] to predict the combustion in spark ignition engines. This combustion model is distinguished by a novel mathematical approach for the hydrogen laminar flame speed calculation, which was implemented through a Gaussian Process Model (GPM). The combustion model was calibrated and validated over the experimental data coming from a 2 L single cylinder engine (SCE), obtaining a good agreement with the experimental results. However, this combustion model has not been validated on engine with a smaller displacement. Krebs et al. [18] presented a multi-zone predictive combustion model for hydrogen combustion in a spark ignition engine with a direct-injection system. The hydrogen-air laminar flame speed is calculated online from the composition of the unburned gas, solving a steady-state reacting flow problem once per cylinder model timestep. This approach would require very high computational costs in the case of carbon-based fuels, whose reaction mechanisms are characterized by a large number of species. The simplicity of hydrogen combustion mechanisms justifies this methodology, but the laminar flame speed model could act as the bottle neck in terms of computational time. According to Krebs et al. a tabulated laminar flame speed model could be useful to reduce the computational times. Moreover, even though reasonable trends were obtained, the work does not provide any comparison with experimental engine data, deferring this assessment to future studies. In Ref. [19], Millo et al. proposed a methodology for evaluating the potential of a hydrogen-powered internal combustion engine by combining zero, one, and three-dimensional (0D/1D/3D) Computational Fluid Dynamics (CFD) approaches. In particular, the SITurb combustion model, developed by Gamma Technologies, was updated with an innovative approach for the laminar flame speed determination. The laminar flame speed was calculated in a 0D-CFD simulation environment (CONVERGE), employing a detailed chemical kinetic mechanism over a large number of engine-relevant operating conditions in terms of

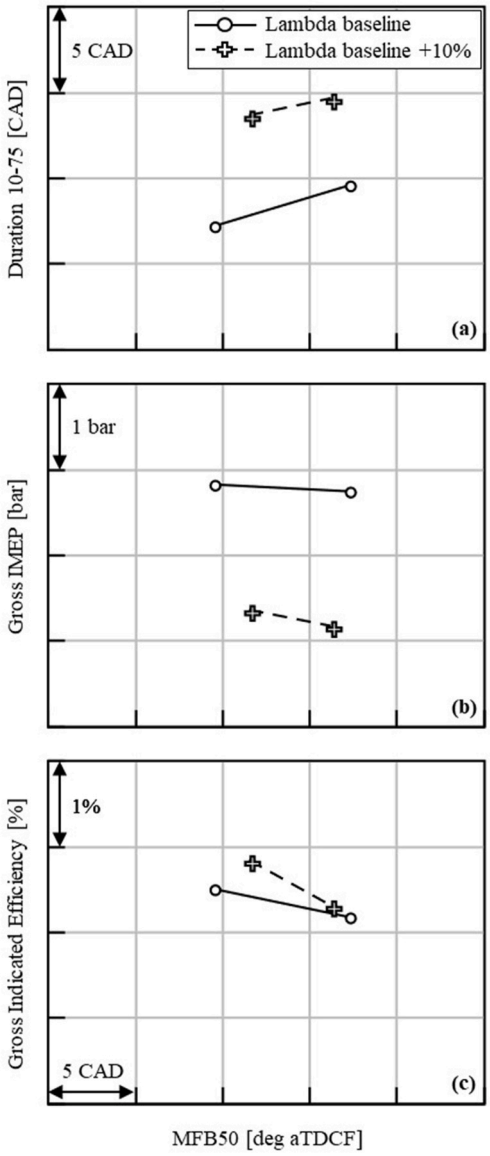

Fig. 3. Experimental data regarding two sweeps of spark advance performed at lambda "baseline" and lambda "baseline" + 10% – full load conditions.

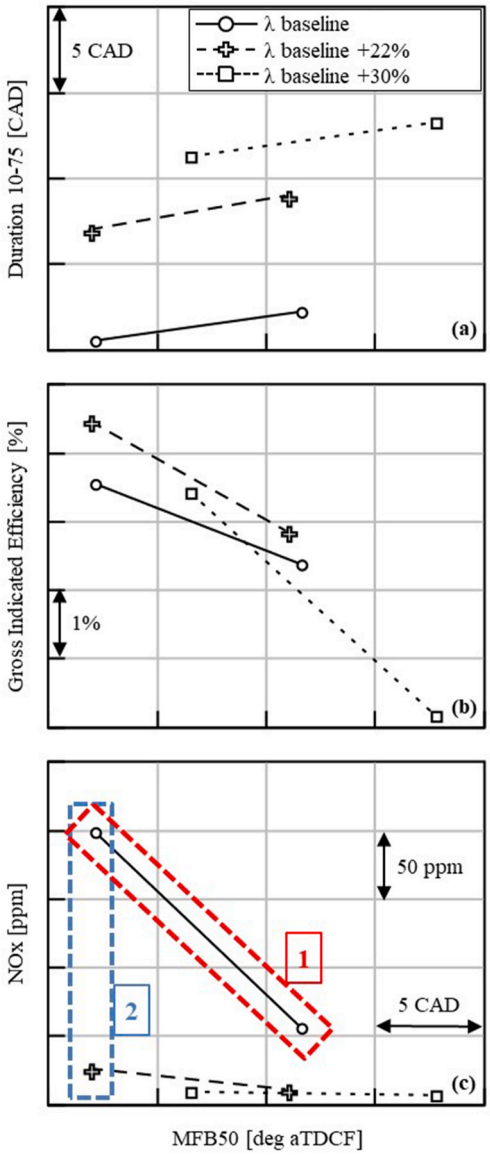

Fig. 4. Experimental data regarding three couples of spark timings performed at lambda "baseline", lambda "baseline" + 22% and lambda "baseline" +30% – partial load conditions.

temperature, lambda, EGR and pressure. Then, the results obtained from the 0D-CFD simulations were integrated into the 0D/1D simulation environment (GT-SUITE) through a correlation function of mixture equivalence ratio capable of fitting detailed chemistry results, accordingly with the approaches proposed in Refs. [14,20]. Since no experimental data for the investigated engine were available at that time, the 0D/1D predictive combustion model was calibrated basing on the results from 3D-CFD combustion simulations, in which the SAGE detailed chemistry combustion model [21] was employed.

In this framework, the present research study aims at improving the accuracy of the previously developed combustion model [19] through a novel approach for the definition of the hydrogen-air flame speed, leveraging also to the availability of experimental data coming from a hydrogen-fuelled 0.5L single-cylinder engine with a port fuel injection (PFI) configuration. Indeed, a dedicated experimental activity was conducted to support the validation of the combustion model considering variation of mixture composition, dilution and phasing of the combustion process. Eventually, the results obtained from the combustion model with the novel approach for laminar flame speed determination showed high accuracy in predicting the combustion process even considering the wide range of thermodynamic and mixture composition conditions under investigation. The findings of this study build upon previous studies by introducing a more comprehensive, time-efficient, and accurate method for predicting the combustion process, accounting for hydrogen-air mixture detailed chemistry. This work lays the groundwork for the development of comprehensive models capable of predicting not only the combustion process, but also the cycle-to-cycle variability and the knock tendency under various engine operating conditions.

2. Case study

The research activity described in this paper relies on experimental data coming from a hydrogen spark-ignited single cylinder engine with a port fuel injection (PFI) configuration, designed by Dumarey. The engine is representative of the retrofitting of a state-of-the-art low compression ratio diesel engine designed for light duty applications. Diesel architectures provide better resistance to hydrogen infiltration [22], thanks to the rugged heavy-duty mission for which they have been

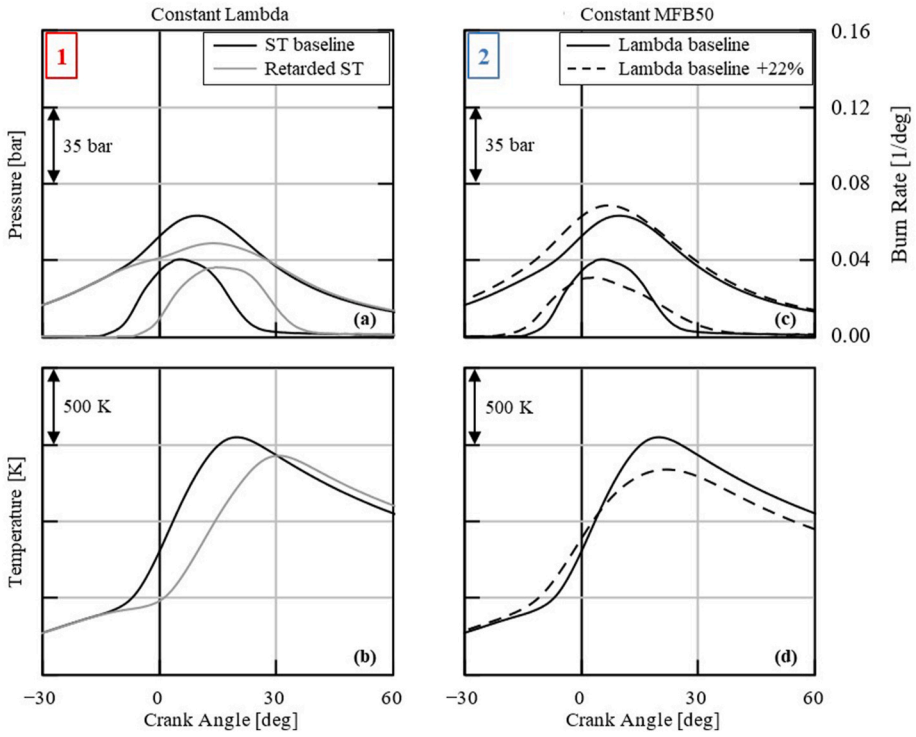

Fig. 5. Experimental pressure cycle and burn rate: (1) – different spark timing, constant lambda; (2) – different lambda, constant MFB50.

designed and withstands high peak firing pressures typical of highly boosted lean strategies better than traditional SI engines. For these reasons, diesel engines are particularly suitable to the adaptation to hydrogen functioning through retrofitting techniques. In this case, the original central diesel injector was replaced by a spark plug without any substantial modification of the original cylinder head. In addition, the diesel piston bowl was replaced with a hemi-spherical bowl. The cylinder head, the intake manifold, and the piston have been specifically machined through additive manufacturing techniques [12]. EGR was controlled through a high-pressure recirculation circuit, equipped with a water-cooled radiator.

The pressure in the intake and the exhaust plenums were controlled to reproduce a compressor-turbine matching without employing an actual turbocharger. This approach aimed to replicate different compressor/turbine configurations of interest and to set boosting and back-pressure to the appropriate levels, thereby exploring the hydrogen combustion properties across a wide range.

The main characteristics of the engine are reported in Table 1.

The engine performances were evaluated under two different load levels at 2000 RPM: the rated torque, critical due to high knock tendency, and a medium-load engine operating condition (i.e., 6 bar BMEP). Since hydrogen can operate with very lean mixtures, the engine run unthrottled during the testing phase for both the engine operating conditions under investigation.

A wide experimental campaign was carried out, considering several variations in terms of lambda, boost pressure, spark timing and EGR, within the limits shown in Table 2. The resulting IMEP720 at full load conditions is included in the range 10–18 bar.

A representation of the combinations of the calibration parameters tested is provided in Fig. 1, where the dimension of each bubble is proportional to the EGR ratio employed.

Only knocking-free operating conditions were considered in this study, with a total of 22 points at full load and 25 points at partial load. For each experimentally tested condition, 100 consecutive cycles have been recorded. Despite the lean operations, the IMEP (Indicated Mean Effective Pressure) variation coefficient was lower than 3% for all the investigated points. The experimental average pressure cycle, which can be considered as representative of the combustion process, was used as reference for the predictive combustion model calibration and validation phases. More details about the engine, the test cell layout, and the experimental campaign can be found in Ref. [12].

3. Experimental data analysis

The experimental data were analyzed to evaluate and, if possible, to separate the effects of each calibration parameters swept (i.e., spark timing, boost pressure, lambda and EGR percentage) on the hydrogen combustion and the engine performance. It is worth to note that variations in engine performances are caused by the impact of the calibration parameters not only on the combustion process, but also on gas exchange losses (for instance, usage of high-pressure cooled EGR can be beneficial due to the pumping mean effective pressure reduction [23]). For this reason, gross quantities, such as the gross IMEP and the gross indicated efficiency, have been used since they focus on the thermodynamics of combustion, while ignoring the variations in terms of gas exchange, which also depend on the selected engine subsystems. The analysis considered only knocking-free operating conditions, defined as those characterized by a percentage of knocking cycles lower than 3%. Therefore, the impact of a calibration parameter on the experimental results such as the combustion duration and the MFB50 is determined solely by variations of the front flame speed, and not by the effects of the knock occurrence.

Fig. 2 depicts the combustion duration (a), the gross IMEP (b), and the gross indicated efficiency (c), for two sweeps of spark advance tested at different EGR levels at full load engine operating condition. The boost pressure and the intake manifold temperature were kept constant during these tests, as well as the air-to-fuel ratio. Moreover, the spark timing was gradually advanced until it reached the knock limit spark advance (KLSA) condition. As the spark timing is advanced, the combustion duration decreases due to the more favorable conditions for the flame propagation, for both the EGR levels. However, the usage of EGR allows water vapor to be recirculated in the cylinder, increasing the specific

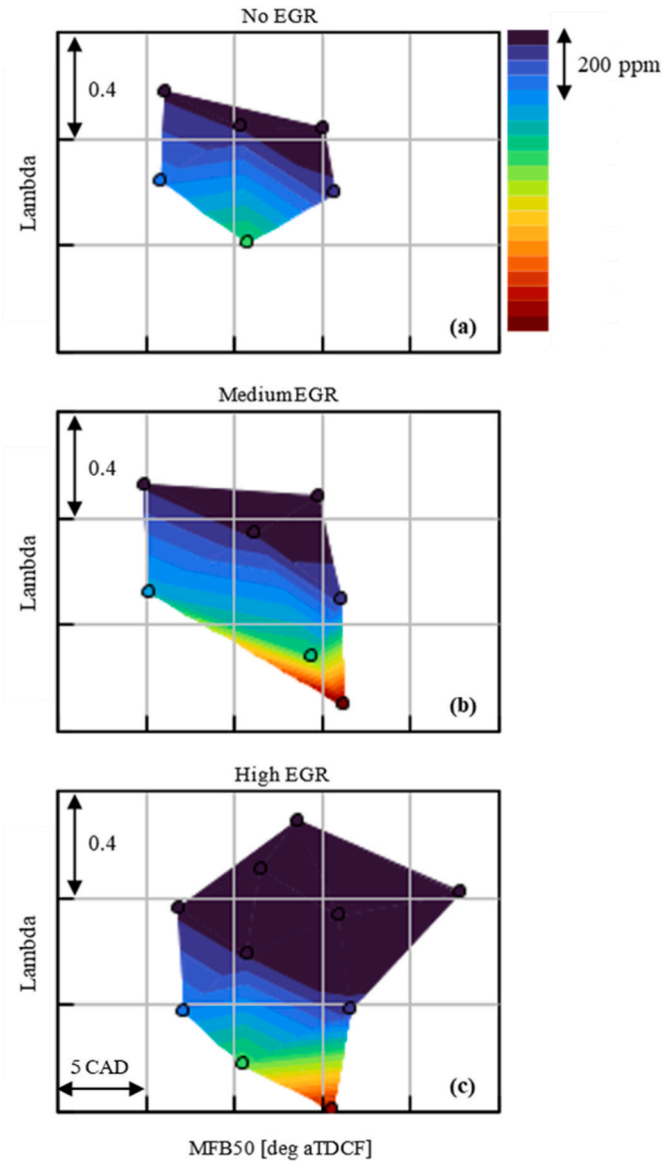

Fig. 6. NOx emissions at partial load conditions under three different levels of EGR, for several combinations of lambda and MFB50.

Table 3
Simulation matrix for the 1D-CFD detailed chemistry laminar flame speed calculations.

	Minimum	Maximum
Equivalence ratio [−]	0.2	1
Unburned temperature [K]	600	1100
Pressure [bar]	10	160
Burned Gas Content [%]	0	30

heat capacity of the mixture, and resulting in lower mixture temperatures [24], thus mitigating knock likelihood by reducing the mixture reactivity and allowing more advanced combustion phasing. It is worth to point out that the gross IMEP for the sweep exploiting higher EGR rate is lower than the baseline case due to the lower amount of hydrogen trapped within the cylinder and the slower combustion (~7 deg difference in terms of MFB1075, as shown in Fig. 2(a)) resulting from the EGR usage. Moreover, even though the lower thermal losses thanks to the EGR usage, the sweep of spark timing performed at the higher EGR level is characterized by a lower gross indicated efficiency (Fig. 2(c)) mainly due to the longer combustion duration.

Fig. 3 depicts the combustion duration (a), the gross IMEP (b), and the gross indicated efficiency (c), for two spark advance sweeps performed at different levels of lambda under full load conditions. These tests have been carried out keeping constant the boost pressure and the EGR fraction. Also in this case, a reduction of the mixture reactivity due to an increase of the air-to-fuel ratio reduces the knock likelihood, allowing advanced spark timing with similar combustion anchor angle. However, since lambda is controlled by the amount of hydrogen injected, the lower amount of fuel for the high air-to-fuel ratio case leads to lower gross IMEP values, as shown in Fig. 4(b). This means that at full load condition, the increment of efficiency thanks to lean operation counterbalances only partially the reduction of available fuel energy within the combustion chamber. Last but not least, even considering the lower laminar flame speed at leaner operations [7], which leads to longer combustion durations (a), similar MFB50 are achieved thanks to the more advanced spark timings. This latter leads therefore to a slightly increase of the gross indicated efficiency (c) also thanks to the lower thermal losses of leaner operations.

As far as partial load condition is concerned, three spark advance sweeps performed at three different lambda levels are depicted in Fig. 4, where the combustion duration (a), the gross indicated efficiency (b) and the engine-out NOx emissions (c) are shown. In these tests the same EGR rate was employed. Differently from full load condition tests, at partial load the engine load was targeted by varying the injected hydrogen, therefore, except for a variation of the engine efficiency, sweeping lambda corresponds to a boost pressure modification. As expected, increasing the mixture dilution leads to longer combustion durations (a). However, if the combustion phasing is kept constant (by advancing the spark timing), the impact of the lower thermal losses related to the lower in-cylinder temperature prevails, resulting in higher indicated efficiencies at higher lambda.

In addition, mixture enleanment is highly beneficial for NOx emissions mitigation as illustrated by Fig. 4 (c). Moreover, also the combustion phasing has an impact on NOx emission at constant mixture composition, however its efficacy is less pronounced for highly diluted mixtures, since the in-cylinder temperatures had already been lowered by the mixture enleanment. These results are consistent with the available literature [22,23].

The impacts of dilution and combustion phasing can also be assessed through the examination of the pressure traces and the average in-cylinder gas temperature profiles shown in Fig. 5. Precisely, two conditions characterized by the different spark timings at the same lambda (red box “1” in Fig. 4(c)), and two conditions with the same combustion phasing but different dilution levels (blue box “2” in Fig. 4(c)) are shown in Fig. 5 left and right, respectively.

The NOx emissions mitigation achieved postponing the spark timing (Fig. 4 (c)) is attributed to the lower in-cylinder temperature due to an unfavorable combustion phasing (Fig. 5 (b)). However, despite the benefits in terms of pollutants emissions, postponing the spark timing is detrimental for the indicted efficiency due to a delayed combustion phasing and a longer burn rate (Fig. 4(a and b)).

As abovementioned, an alternative approach to mitigate the NOx could be the increment of air-to-fuel ratio. In this scenario, advancing the spark timing is necessary to keep the same MFB50, due to the longer combustion duration given by the leaner mixtures. The increase of trapped air within the cylinder leads to higher pressure levels (Fig. 5 (c)), but the diluting effect allows reducing the in-cylinder temperature (Fig. 5 (d)), thereby reducing the NOx emissions (Fig. 4 (c)), and being beneficial for the gross indicated efficiency due to the lower thermal losses (Fig. 4 (b)).

An alternative solution to air-to-fuel and combustion phasing aiming at reducing engine-out NOx emissions reduction is the exploitation of EGR. Fig. 6 provides an assessment of the influence of these three parameters on the NOx emission at partial load engine operating condition. It shows the NOx emissions as a function of the air-to-fuel ratio and

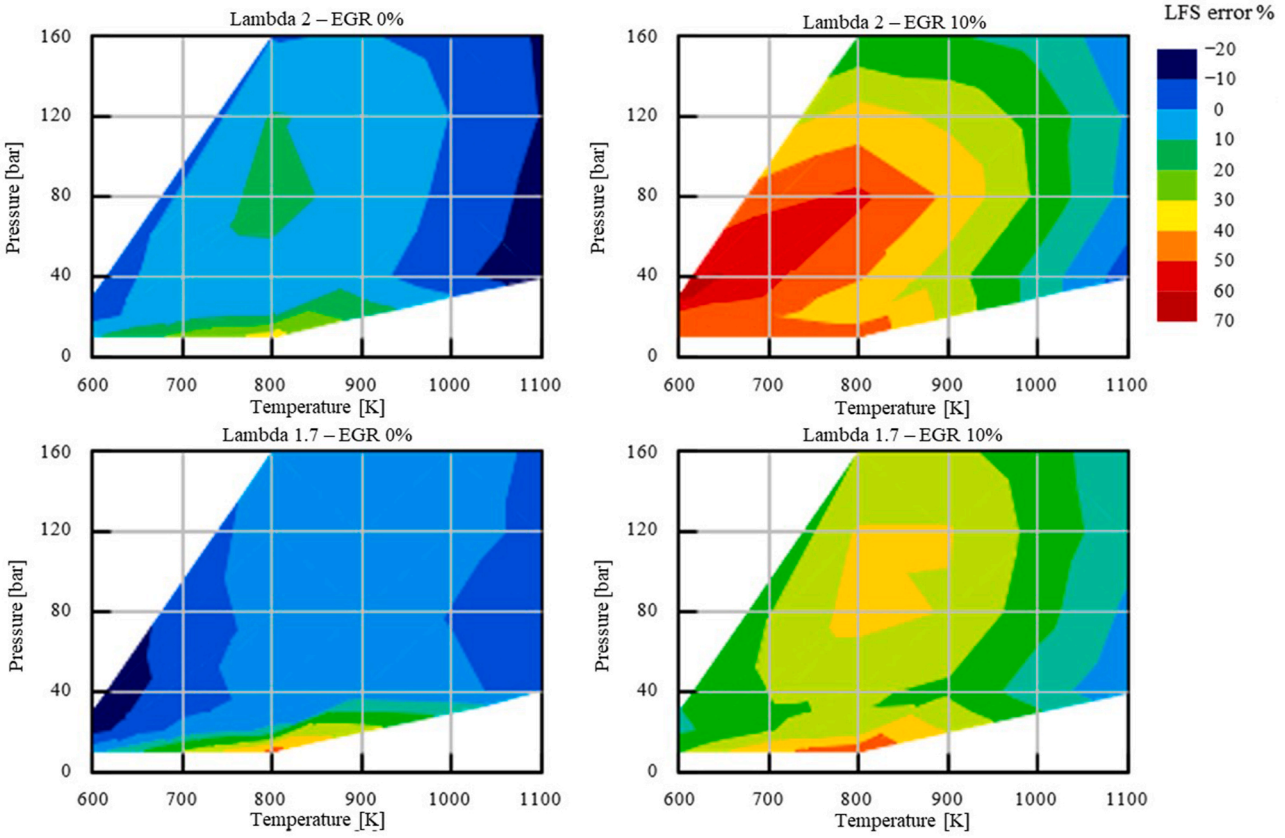

Fig. 7. Laminar flame speed percentage difference between 1D detailed chemistry calculations (reference) and polynomial correlation for different mixture conditions (lambda, EGR, pressure and temperature).

the MFB50 for three distinct levels of EGR rate. High dilution levels contributed to achieve ultra-low NOx emissions (<50 ppm), consistently with other experimental results already available in literature [11,25]. Furthermore, retarding the combustion timing while retaining the same mixture composition leads to a NOx emission reduction. However, the impact of the air-to-fuel ratio on the NOx emissions is largely more significant in comparison with the combustion phasing.

The analysis of the experimental campaign in terms of the different impact of each calibration variable on performance and emissions has been considered preparatory for the development of a predictive combustion model, since the understanding of the impact of each calibration parameters at different engine operating conditions is crucial for the validation of the proposed model.

4. Combustion model

The SITurb predictive combustion model, already accessible in the commercially available software GT-SUITE, was used as the basis for the developed hydrogen combustion model. The SITurb is a phenomenological two-zone model, widely used for gasoline homogeneous charge spark ignition engines [16,17]. It is based on a traditional entrainment and burn-up approach in which the turbulent flame propagation is initiated from a fixed location (i.e., spark) within the cylinder. Before the spark timing, the in-cylinder mass is contained into a single thermodynamic zone, the unburned zone. Once the combustion starts triggered by the spark, the flame front starts propagating from the spark location towards the combustion chamber walls, assuming an ideal spherical propagation. During the flame propagation, the homogeneous mixture is progressively entrained into the flame front accordingly to the entrainment rate, calculated in Eq. (1).

$$\frac{dM_e}{dt} = \rho_u A_f (S_T + S_L) \quad \text{(Eq.1)}$$

Where M_e is the mixture entrained mass, A_f is the flame area, ρ_u unburned gas density, S_L the laminar flame speed and S_T the turbulent flame speed.

The speed up of flame propagation due to the flame wrinkling is taken into account computing the turbulent flame speed as shown in Eq. (2).

$$S_T = C_{TFS} u' \left(1 - \frac{1}{1 + C_{FKG} \left(\frac{R_f}{L_T} \right)^2} \right) \quad \text{(Eq.2)}$$

Indeed, the turbulent flame speed computation depends, besides from the flame radius (R_f) and the turbulence integral length scale (L_T), on the turbulent intensity (u'). C_{TFS} and C_{FKG} are tuning parameters to adjust both the flame velocity and the initial growth rate of the flame kernel, respectively. It is worth to note that during the flame kernel growth phase, the laminar flame speed governs the entrainment rate. This occurs because the flame radius is too small to make the flame wrinkling effects negligible during the early stages of the combustion.

The rate at which mass is transferred into the burned zone, known as the burn rate, is calculated in Eq. (3).

$$\frac{dM_b}{dt} = \frac{M_e - M_b}{\tau} \quad \text{(Eq.3)}$$

M_b is the mixture burned mass. It is proportional to the amount of unburned mixture behind the flame front, $M_e - M_b$, divided by a characteristic burning timescale τ, that represents the time needed by the laminar flame speed to cover the Taylor microscale of turbulence (λ). τ is

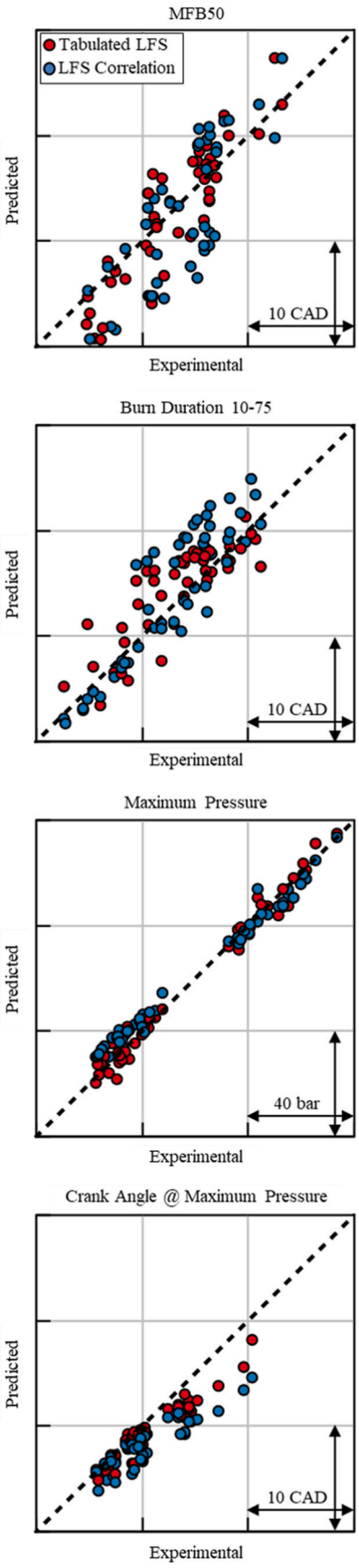

Fig. 8. Correlation plots for combustion anchor angle (MFB50), combustion duration (MFB10-75), maximum in-cylinder pressure (Maximum Pressure) and its crank angle (Crank Angle @ Maximum Pressure).

Table 4
Root Mean Square Errors (RMSE) on combustion and pressure-related parameters resulting from SITurb model optimizations.

	Root Mean Square Error (RMSE)	
	LFS correlation	Tabulated LFS
MFB50 [CAD]	4.8	3.0
Burn Duration 10–75 [CAD]	3.4	2.7
Maximum Pressure [bar]	5.2	4.0
CA @ Max. Pressure [CAD]	2.7	1.7

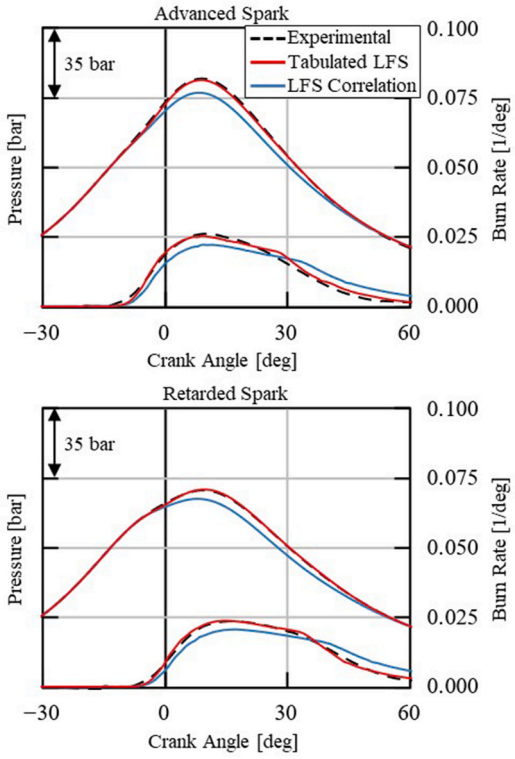

Fig. 9. Experimental (black dashed), predicted with LFS correlation (red), and predicted with tabulated LFS (blue) average in-cylinder pressure and burn rate for two different conditions of spark timing at the same lambda, boost pressure and EGR (full load). (For interpretation of the references to color in this figure legend, the reader is referred to the Web version of this article.)

calculated by Eq. (4).

$$\tau = \frac{\lambda}{S_L} \quad \text{(Eq.4)}$$

The Taylor microscale of turbulence λ is defined as in Eq. (5), where Re_t is the Reynolds number and C_{TLS} is a tuning parameter.

$$\lambda = C_{TLS}\frac{L_T}{\sqrt{Re_t}} \quad \text{(Eq.5)}$$

As it can be noticed, the combustion model relies on the turbulent kinetic energy and the integral length scale. These quantities are calculated by a predictive in-cylinder turbulence model based on the K-k-eps approach [26]. The employed turbulence model was properly calibrated to match the 3D-CFD simulation results.

As far as laminar flame speed is concerned, two different user subroutines have been defined: the first one based on a mathematical correlation, the second based on LFS tables. Both approaches rely on the detailed chemistry 1D-CFD computations carried out considering wide ranges of pressure, temperature, equivalence ratio and residual gasses, representative of engine-relevant conditions. The detailed Zhang et al.

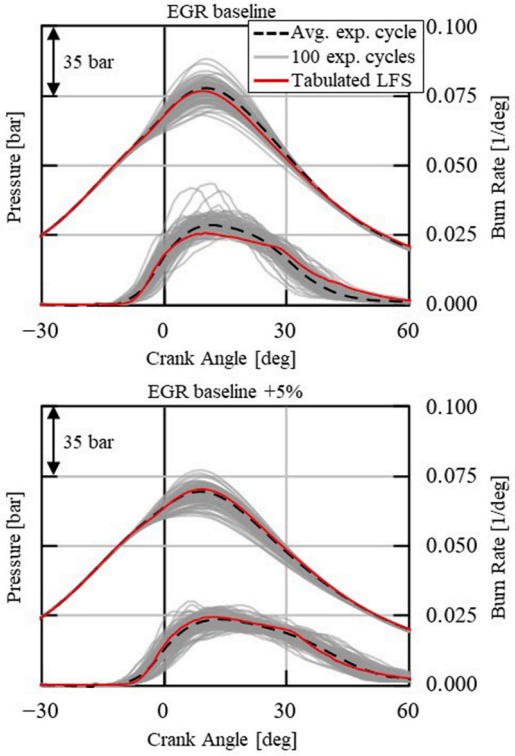

Fig. 10. Experimental (black dashed) and predicted (red) average in-cylinder pressure and burn rate; 100 experimental consecutive cycles (grey). Two different EGR conditions at same lambda, boost pressure and spark timing (full load). (For interpretation of the references to color in this figure legend, the reader is referred to the Web version of this article.)

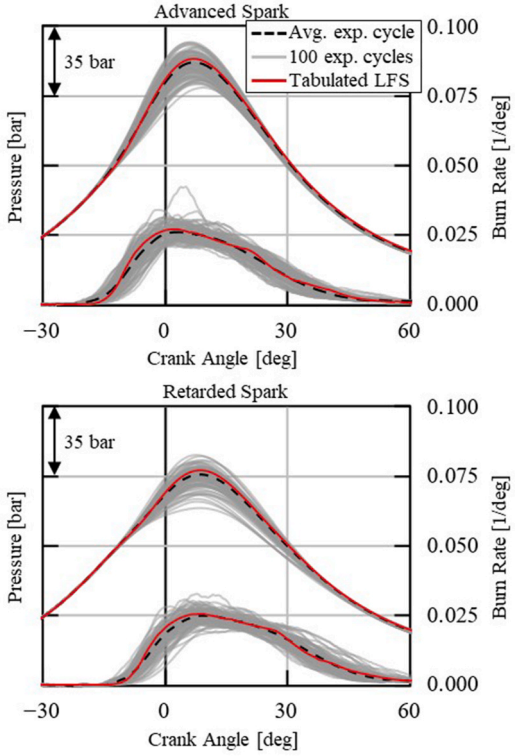

Fig. 11. Experimental (black dashed) and predicted (red) average in-cylinder pressure and burn rate; 100 experimental consecutive cycles (grey). Two different spark timings at same lambda, boost pressure and EGR (full load). (For interpretation of the references to color in this figure legend, the reader is referred to the Web version of this article.)

mechanism [26] was used as reaction scheme for hydrogen oxidation. The simulation matrix is reported in Table 3, resulting in more than 1600 different operating condition.

The laminar flame speed model based on the correlation function was inherited from the work described in Ref. [19]. Specifically, the correlation function employed was defined consistently with [20], as shown in Equation (6).

$$S_L(\Phi, T_u, p_u, x_b) = S_{L0}\left(\frac{T_u}{T_0}\right)^{\alpha}\left(\frac{p_u}{p_0}\right)^{\beta}(1-\gamma x_b) \quad \text{(Eq.6)}$$

S_{L0} is the laminar flame velocity evaluated at the reference conditions ($T_U = T_0 = 298$ K; $p_U = p_0 = 1$ atm; residual gas fraction $x_b = 0$), while α, β, and γ are coefficients that quantify the sensitivity of the laminar flame speed to the unburned gas pressure, temperature, and residual gas fraction, respectively. The S_{L0} is defined accordingly with the approach proposed by Verhelst and Sierens [20], where a fifth-order polynomial function of the equivalence ratio Φ is used to describe the laminar flame speed in reference operating conditions, as in Equation (7).

$$S_{L0}(\Phi) = 30.009\Phi^5 - 87.697\Phi^4 + 88.628\Phi^3 - 33.781\Phi^2 + 5.489\Phi - 0.301 \quad \text{(Eq.7)}$$

Similarly, the coefficients α, β, and γ of Equation (6) were defined using second-order polynomial expressions dependent on the equivalence ratio, as reported in Equations (8)–(10).

$$\alpha = 0.105\Phi^2 - 3.135\Phi + 6.514 \quad \text{(Eq.8)}$$

$$\beta = 0.177\Phi^2 + 0.636\Phi - 1.449 \quad \text{(Eq.9)}$$

$$\gamma = -0.306\Phi^2 + 0.418\Phi + 2.134 \quad \text{(Eq.10)}$$

The coefficients of each polynomial expression were properly calibrated to minimize the differences between the correlation results (Eq. (6)) and the 1D-CFD detailed chemistry calculations. Fig. 7 shows the percentage error between the laminar flame speed correlation and the results from the detailed chemistry calculations, as a function of the in-cylinder pressure and the unburned gas temperature, for different mixture dilution and compositions. The error is computed having as a reference the 1D results from the detailed chemistry calculations.

Adopting the described mathematical correlation, although a satisfactory agreement was achieved for large sweeps of pressure and temperature, a not negligible overprediction can be highlighted especially when EGR is exploited. More specifically, the second column is referred to EGR = 10% mixture condition and highlights up to 70% LFS overprediction, thus being potential source of error in the combustion process prediction. Due to this reason, in this study a novel approach was considered to minimize the error with the laminar flame speed detailed chemistry calculations, being the laminar flame speed fundamental for the model accuracy, as shown in Eq. (1) and Eq. (4). More specifically, the laminar flame speed model was implemented in GT-SUITE by means of several look-up tables containing the results of the detailed chemistry calculations. The tabulated approach enabled by a dedicated user subroutine provides the value of LFS at each timestep depending on pressure, temperature, equivalence ratio and residual gas fraction in the cylinder.

5. Results

As previously described, the combustion model requires the tuning of three calibration constants (i.e., C_{TFS} C_{FGK} and C_{TLS}). Therefore, an optimization process has been employed in GT-SUITE basing on the NSGA-III genetic algorithm (GA) [27]. This algorithm is extensively utilized for optimizing predictive combustion models [17,28], as it is

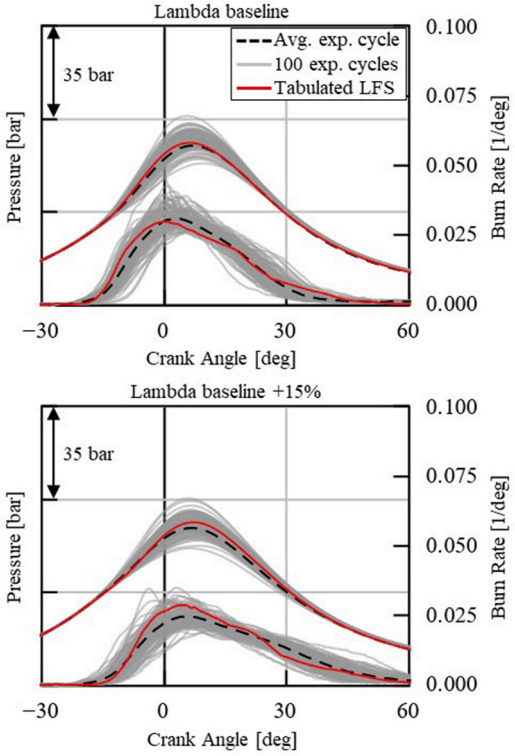

Fig. 12. Experimental (black dashed) and predicted (red) average in-cylinder pressure and burn rate; 100 experimental consecutive cycles (grey). Two different lambda values at same boost pressure, EGR and spark timing (partial load). (For interpretation of the references to color in this figure legend, the reader is referred to the Web version of this article.)

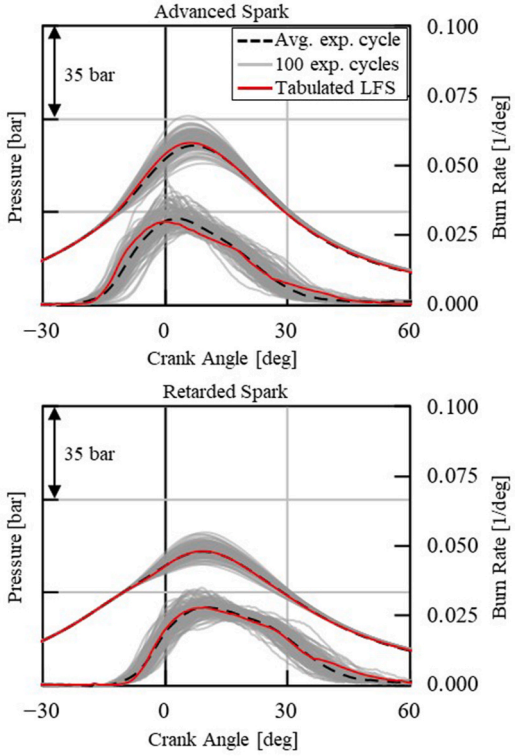

Fig. 13. Experimental (black dashed) and predicted (red) average in-cylinder pressure and burn rate; 100 experimental consecutive cycles (grey). Two different spark timings at same lambda, boost pressure and EGR (partial load). (For interpretation of the references to color in this figure legend, the reader is referred to the Web version of this article.)

particularly effective for multi-modal problems of medium to high complexity. In particular, it is less likely to become trapped in local minimum compared to other optimization tools provided by GT-SUITE, thereby increasing the probability of reaching the global optimum solution [29]. As objective for the optimization process, the root mean squared error between the measured and the simulated burn rate was minimized, keeping unchanged the three calibration parameters moving from an engine operating condition to another. Moreover, to increase the reliability of the model, without inducing any bias from the selection of the training dataset, 16 operating conditions were randomly selected among the full load and partial load datasets to cover a wide range of lambda, EGR and spark timings, and they were used as training dataset. Therefore, the combustion model was validated over the remaining 31 operating conditions. In addition, the calibration procedure was performed for both the laminar flame speed models previously mentioned to highlight pros and cons of each approach and select the most reliable one.

The correlation plots of MFB50, Burn Duration 10–75 (combustion-related parameters) and Maximum Pressure, CA of Maximum Pressure (pressure-related parameters) resulting from the optimization process are shown in Fig. 8, where each circle represents a single operating condition, and the color identifies the LFS model employed (i.e., red – tabulated approach, blue – polynomial correlation). Generally, the tabulated laminar flame speed model leads to a better correlation with the experiments, since most of the points are much closer to the zero-error line, highlighted with the black dashed line.

To quantify the correlation level, the root mean square errors both for combustion and pressure-related parameters were computed and are shown in Table 4. Even if both models provide a more than satisfactory accuracy, the tabulated LFS approach shows lower errors demonstrating the better predictive capabilities compared to the polynomial correlation. Indeed, thanks to this approach, the combustion duration and the maximum in-cylinder pressure average errors are lower than 3 deg and 4 bar, respectively.

A further comparison between the results obtained from the two approaches for the LFS determination is given in Fig. 9, where a sweep of spark timing at full load conditions was analyzed. In particular, the average in-cylinder pressure trace and the respective burn rate obtained from simulations were compared with the experimental data. Also in this case, the LFS model with the tabulated approach better matches the experimental data, especially as regards the in-cylinder peak pressure and the burn rate shape.

Once assessed the differences among the two LFS models, the results obtained from the combustion model with the tabulated laminar flame speed were further analyzed since it provided more accurate predictions. Simulations results were compared with the experimental data considering different variations of EGR percentage, boost pressure (lambda) and spark timing in Figs. 10–12, and Fig. 13. Generally, a very good agreement between the experimental traces and the predicted ones was observed, both at full load and partial load. The combustion model demonstrates to be able to properly calculate the burn rate varying spark timing and dilutions levels, both in terms of lambda and EGR, leading to a very good match between the results from the simulation and the experimental data.

The assessment of the combustion model capabilities was finally carried out comparing the combustion model results in terms of combustion phasing (MFB50) with the experimental data considering several sweeps of spark timing, performed under various operating conditions. Two spark timing sweeps carried out at full load with high and low EGR levels are shown in Fig. 14. The experimental data are shown with their respective confidence bands, calculated using a $\pm\sigma$ interval, where σ represents the standard deviation of MFB50. Also in this case, a very good agreement with experimental data was highlighted: the model is able to properly predict the MFB50 over the entire

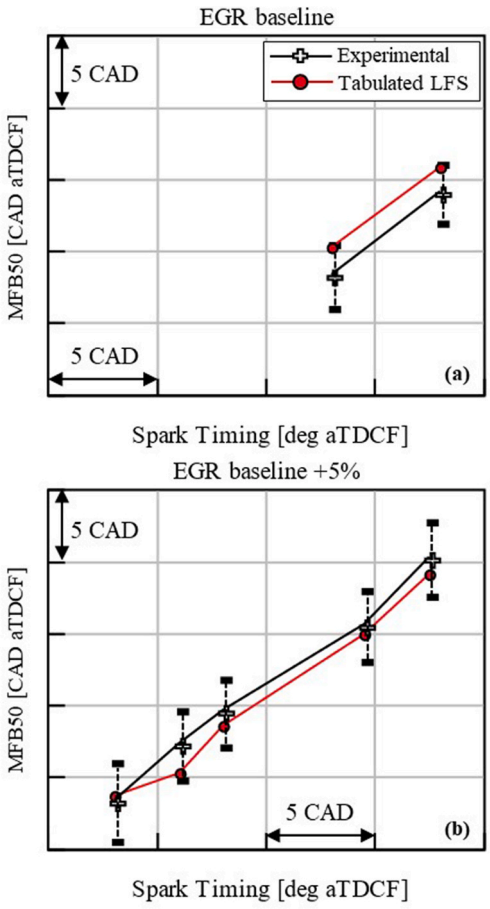

Fig. 14. Experimental (black) and predicted (red) MFB50 and burn duration for two different spark timing sweeps at different EGR levels (full load). (For interpretation of the references to color in this figure legend, the reader is referred to the Web version of this article.)

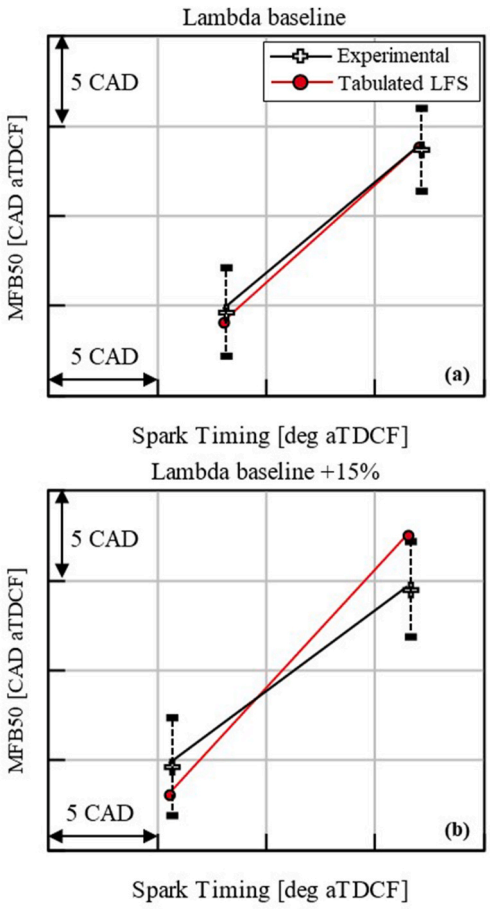

Fig. 15. Experimental (black) and predicted (red) MFB50 and burn duration for two different spark timing sweeps at different lambda levels (partial load). (For interpretation of the references to color in this figure legend, the reader is referred to the Web version of this article.)

sweep of spark timing for both EGR levels, demonstrating its good sensitivity to both EGR and spark timing variations.

The results indicate that the deviation from the MFB50 of the average experimental cycle due to cycle-to-cycle variation is higher than the error of the predictive model. This confirms the model robustness in capturing the average combustion behavior. The correlation of the optimized combustion model with the experimental data was investigated also for partial load operating conditions in Fig. 15. In particular, two spark sweeps at two different lambda values were considered.

The developed predictive combustion model with the tabulated laminar flame speed results to properly estimate the MBF50 for different mixture compositions, confirming its good predictive capabilities also at partial load engine operating conditions. It is worth to point out that a single set of calibration constants has been used avoiding a case-by-case calibration, thus confirming the reliability of the developed model.

The optimized hydrogen combustion model can be combined with a knock model and a cycle-to-cycle variation model to create a comprehensive tool capable of predicting not only the combustion rate, but also the cycle-to-cycle variability, the knock tendency and the percentage of knocking cycles for each operating condition [30].

6. Conclusions

In this study a combustion model is proposed for the prediction of the combustion process of hydrogen fuelled internal combustion engines. The predictive combustion model relies on a novel approach for the determination of the air-hydrogen flame speed, and takes the advantage of a dedicated experimental campaign carried out on a 0.5L single-cylinder engine, retrofitted from a diesel architecture and adapted to the hydrogen functioning. The experimental data, widely used for the validation of the model, include several sweeps of spark timing, lambda, EGR, and boost pressure, performed under full load and partial load operating conditions.

First, the experimental data have been analyzed to evaluate the impact of each calibration parameter on the hydrogen combustion. The analysis revealed that, as expected, calibration parameter variations highly affects the combustion process, making the development of such simulation tool challenging. Starting from this latter and considering hydrogen peculiarities, the air-hydrogen laminar flame speed has been calculated employing a detailed chemistry scheme on a large number of operating conditions in terms of mixture composition, pressure and temperature. The laminar flame speed calculations were implemented considering two different approaches: a polynomial correlation function of mixture composition, and a tabulated approach. The developed combustion model has been calibrated through an optimization process with the NSGA-III Genetic Algorithm on a dataset of 16 operating conditions and validated against the remaining 31 operating points. The combustion model employing the tabulated laminar flame speed provided a more than satisfactory accuracy level, demonstrating a good agreement with the experimental data.

The developed predictive combustion model, which provides an accurate and time-efficient method for simulating the combustion process in hydrogen-fuelled engines, can be further extended in future work through its integration with predictive knock and cycle-to-cycle

variability (CCV) models. This integrated approach allows the development of a comprehensive model capable of predicting not only the combustion process but also the cycle-to-cycle variability and the percentage of knocking cycles under various engine operating conditions. Such a comprehensive model can serve as a highly powerful tool for significantly accelerating the development of hydrogen-fuelled engines.

CRediT authorship contribution statement

Andrea Piano: Writing – review & editing, Visualization, Supervision, Methodology, Conceptualization. **Gianpaolo Quattrone:** Writing – original draft, Visualization, Validation, Investigation. **Federico Millo:** Supervision, Project administration. **Francesco Pesce:** Supervision, Resources, Project administration, Conceptualization. **Alberto Vassallo:** Writing – review & editing, Supervision, Resources, Conceptualization.

Declaration of competing interest

The authors declare that they have no known competing financial interests or personal relationships that could have appeared to influence the work reported in this paper.

References

[1] IEA. Net zero emissions by 2050 scenario (NZE). https://www.iea.org/reports/global-energy-and-climate-model/net-zero-emissions-by-2050-scenario-nze. [Accessed 22 July 2024].

[2] Onorati A, Payri R, Vaglieco BM, Agarwal AK, et al. The role of hydrogen for future internal combustion engines. Int J Engine Res 2022;23(4):529–40. https://doi.org/10.1177/14680874221081947.

[3] Huang Q, Liu J, et al. Preliminary assessment of the potential for rapid combustion of pure ammonia in engine cylinders using the multiple spark ignition strategy. Int J Hydrogen Energy 2024;55:375–85. https://doi.org/10.1016/j.ijhydene.2023.11.136.

[4] Bičáková O, Straka P. Production of hydrogen from renewable resources and its effectiveness. Int J Hydrogen Energy 2012;37:11563–78. https://doi.org/10.1016/j.ijhydene.2012.05.047.

[5] Stępień Z. A comprehensive overview of hydrogen-fueled internal combustion engines: achievements and future challenges. Energies 2021;14. https://doi.org/10.3390/en14206504.

[6] Karim GA. Hydrogen as a spark ignition engine fuel. Int J Hydrogen Energy 2003;28:569–77. https://doi.org/10.1016/S0360-3199(02)00150-7.

[7] Sun D, Liu F. Research on the performance and emission of a port fuel injection hydrogen internal combustion engine. International conference on computer distributed control and intelligent environmental monitoring. CDCIEM; 2011. p. 963–6. https://doi.org/10.1109/CDCIEM.2011.523. 2011.

[8] Schefer RW, White C, Keller J. Lean combustion. 2008. p. 213–54. https://doi.org/10.1016/B978-012370619-5.50009-1. ISBN: 9780123706195.

[9] Pauer T, Weller H. Hydrogen engines for future passenger cars and light commercial vehicles. MTZ Worldwide 2021;82:42–7. https://doi.org/10.1007/s38313-020-0603-1.

[10] Ozdor N, Dulger M, Sher E. An experimental study of the cyclic variability in spark ignition engines. Reprinted from: Advances in Engine Combustion and Flow Diagnostics, SAE Technical Paper, 1996-02–01 1996. https://doi.org/10.4271/960611.

[11] Sementa P, de Vargas Antolini JB, Tornatore C, Catapano F, et al. Exploring the potentials of lean-burn hydrogen SI engine compared to methane operation. Int J Hydrogen Energy 2022;47:25044–56. https://doi.org/10.1016/j.ijhydene.2022.05.250.

[12] Buzzi L, Biasin V, Galante A, Gessaroli D, et al. Experimental investigation of hydrogen combustion in a single cylinder PFI engine. THIESEL 2022 conference on thermo- and Fluid Dynamics of clean propulsion powerplants. 2022. https://doi.org/10.4271/2022-01-0331.

[13] Yip HL, Srna A, Yuen ACY, Kook S, et al. A review of hydrogen direct injection for internal combustion engines: towards carbon-free combustion. Appl Sci 2019;9. https://doi.org/10.3390/app9224842.

[14] D'Errico G, Onorati A, Ellgas S. 1D thermo-fluid dynamic modelling of an S.I. single-cylinder H2 engine with cryogenic port injection. Int J Hydrogen Energy 2008;33:5829–41. https://doi.org/10.1016/j.ijhydene.2008.05.096.

[15] Rezaei R, Hayduk C, Fandakov A, Rieß M. Numerical and experimental investigations of hydrogen combustion for heavy-duty applications. SAE Technical Paper, 2021-01-0522 2021. https://doi.org/10.4271/2021-01-0522.

[16] Millo F, Gullino F, Rolando L, et al. Methodological approach for 1D simulation of port water injection for knock mitigation in a turbocharged DISI engine. Energies 2020;13(17):4297. https://doi.org/10.3390/en13174297.

[17] Mirzaeian M, Millo F, Rolando L, et al. Assessment of the predictive capabilities of a combustion model for a modern downsized turbocharged SI engine. SAE technical papers, 2016-01–0557. 2016. https://doi.org/10.4271/2016-01-0557.

[18] Krebs S, Biet C. Predictive model of a premixed, lean hydrogen combustion for internal combustion engines. Transport Eng 2021;5. https://doi.org/10.1016/j.treng.2021.100086.

[19] Millo F, Piano A, Rolando L, Accurso F, et al. Synergetic application of zero-, one-, and three-dimensional computational fluid Dynamics approaches for hydrogen-fuelled spark ignition engine simulation. SAE International Journal of Engines 2021;15. https://doi.org/10.4271/03-15-04-0030.

[20] Verhelst S, Sierens R. A Laminar burning velocity correlation for hydrogen/air mixtures valid at Spark-Ignition engine conditions. Spring technical conference of the ASME internal combustion engine division. 2003. https://doi.org/10.1115/ICES2003-0555.

[21] Convergent Science. "CONVERGE Manual v3.0.". 2020.

[22] Azeem N, Beatrice C, Vassallo A, Pesce F, et al. Review and assessment of the material's compatibility for rubbers and elastomers in hydrogen internal combustion engines. SAE Technical Paper 2022. https://doi.org/10.4271/2022-01-0331.

[23] Thomas Koch D, Sousa A, Bertram D. H2-Engine operation with EGR achieving high power and high efficiency emission-free combustion. SAE Technical Paper, 2019-01–2178 2019. https://doi.org/10.4271/2019-01-2178.

[24] Chaichan MT. EGR effects on hydrogen engines performance and emissions. Int J Sci Eng Res 2016;7(3):80–90.

[25] Bao L, zhi, Sun, gang B, Luo, he Q. Experimental investigation of the achieving methods and the working characteristics of a near-zero NOx emission turbocharged direct-injection hydrogen engine. Fuel 2022;319. https://doi.org/10.1016/j.fuel.2022.123746.

[26] Zhang K, Banyon C, Bugler J, Curran HJ, et al. An updated experimental and kinetic modeling study of n-heptane oxidation. Combust Flame 2016;172:116–35. https://doi.org/10.1016/j.combustflame.2016.06.028.

[27] Deb K, Jain H. An evolutionary many-objective optimization algorithm using reference-point-based nondominated sorting approach, Part I: solving problems with box constraints. IEEE Trans Evol Comput 2014;18:577–601. https://doi.org/10.1109/TEVC.2013.2281535.

[28] Accurso F, Piano A, Millo F, Caputo G, et al. Numerical simulation of a prechamber-ignited lean-burn gas engine by means of predictive combustion models. SAE International Journal of Engines 2023;16(5):623–41. https://doi.org/10.4271/03-16-05-0037.

[29] Gamma Technologies. "GT-SUITE reference manual". 2022.

[30] Piano A, Millo F, Quattrone G, Pesce F, et al. Comprehensive quasi-dimensional model to predict combustion process, knock likelihood and cycle-by-cycle variability in a hydrogen-fueled internal combustion engine. JSAE/SAE Powertrains, Energy and Lubricants International Meeting 2023;2023–32–0171. https://doi.org/10.4271/2023-32-0171.